RES MILITARIS
REVUE EUROPEENNE D ETUDES EUROPEAN JOURNAL OF MILITARY STUDIES
Social Science Journal

Innovative Image-Guided Synthesis Identifies Histone Deacetylase Inhibitors with Enhanced Blood-Brain Barrier Penetration

1PRASAD PINNOJU,2RAVI KIRAN KOMALLA
12Assistant Professor
DEPT of H&S
Vaagdevi College of Engineering, Warangal, TS, India

ABSTRACT:

This research presents an innovative image-guided synthesis approach to identify potent histone deacetylase inhibitors (HDACi) with enhanced permeability across the blood-brain barrier (BBB). By leveraging imaging techniques, we systematically screened a library of compounds to pinpoint those capable of effectively penetrating the BBB. Our findings reveal several novel HDAC inhibitors that demonstrate significant therapeutic potential for central nervous system disorders. This study not only advances the understanding of HDAC inhibition but also highlights the importance of targeted synthesis methodologies in developing drug candidates that can successfully navigate the challenges of brain delivery.

KEYWORDS: Benzamides, blood-brain barrier permeability, positron emission tomography, and histone deacetylase.

INTRODUCTION

The blood-brain barrier (BBB) serves as a crucial protective shield for the central nervous system (CNS), regulating the passage of substances between the bloodstream and brain tissue. While this barrier is essential for maintaining neuronal homeostasis, it also poses significant challenges for drug delivery, particularly for therapeutic agents targeting neurological disorders. Among these agents, histone deacetylase inhibitors (HDACi) have garnered attention for their potential to modulate gene expression and exert neuroprotective effects. However, the effective delivery of HDAC inhibitors across the BBB remains a major hurdle in their clinical application.

Recent advances in imaging technologies have opened new avenues for drug discovery, allowing for the identification and optimization of compounds with favorable pharmacokinetic properties. By employing image-guided synthesis techniques, researchers can visualize the interactions between compounds and the BBB, facilitating the design of molecules specifically tailored for enhanced permeability. This approach not only streamlines the drug development process but also increases the likelihood of finding effective treatments for CNS conditions.

In this study, we explore the synthesis and characterization of novel HDAC inhibitors capable of crossing the BBB. By integrating imaging methodologies into the synthesis process, we aim to uncover compounds that exhibit potent HDAC inhibition alongside favorable BBB permeability. This investigation not only aims to enhance our understanding of HDAC inhibition in the context of CNS disorders but also to contribute to the broader field of targeted drug delivery strategies.

The subsequent sections will detail the methods employed in the image-guided synthesis, the evaluation of BBB permeability, and the biological activity of the identified HDAC inhibitors. Through this work, we hope to provide insights into the design of effective

therapeutics for neurological diseases and highlight the potential of image-guided strategies in overcoming the challenges posed by the BBB.

Epigenetic regulation of gene expression via enzymatic modification of DNA and histone proteins is implicated in development,1 inflammation,2 heart disease,3 cancer,4 and neuropsychiatric disorders5,6 including depression, Alzheimer's disease, and substance use disorders. Two common and influential epigenetic transformations are DNA methylation and chromatin modifications, which provide a mechanism for the transmission of environmentally cued information to subsequent generation of cells thereby producing phenotypic diversity without changing DNA sequence. Histone acetyl transferase (HAT) and histone deacetylase (HDAC) are histone modifying enzymes that regulate gene expression by catalyzing the addition and removal of acetyl

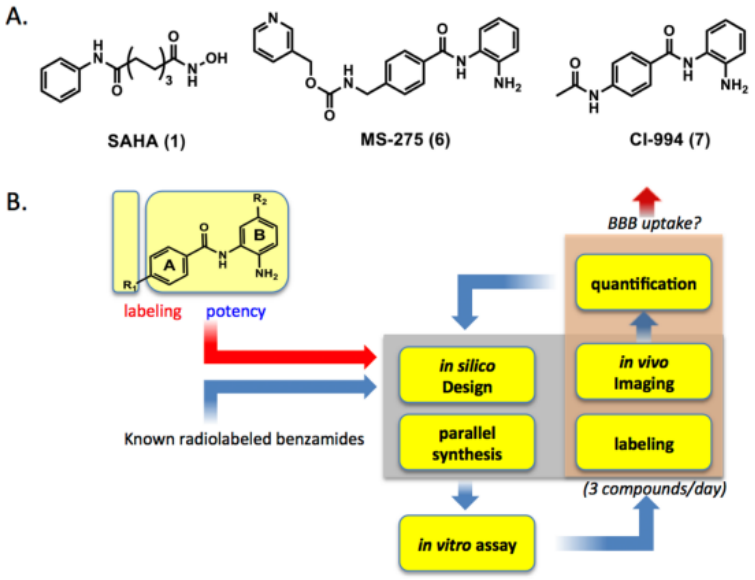

Figure 1. Known HDAC inhibitor drugs (A) and the flowchart for image-guided systematic approach (B).

bunches from the lysine gatherings of histone proteins, which in relationship with DNA structure chromatin. HDAC eliminates an acetyl gathering of histone proteins (by hydrolysis of acetamido gathering of ε-carbon of lysine buildups), instigating a tight charge− charge connection among DNA and histone proteins, subsequently delivering the DNA blocked off to record factor restricting and quelling quality articulation. By and large, histone acetylation is related with enactment of quality articulation presenting DNA to record factors while deacetylation is connected to quality suppression by consolidating the chromatin delivering DNA less accessible for record. There are four classes of HDAC (I, II, III, IV) and 11 isoforms. Class I HDACs (1, 2, 3, 8 subtype) are normally tracked down in the core, while class II HDAC (4, 5, 7, 9 subtype) and class IV (HDAC 11 subtype) happen in both cytoplasm and core. With the exception of Class III HDAC, all HDACs contain a Zn particle in the substrate restricting pocket where the hydrolysis of the acetamide security happens. Class I HDAC inhibitors (HDACi) have been created as possible therapy of diseases. Suberoylanilide hydroxamic corrosive (1, SAHA, Zolinza, Figure 1A) was supported as the primary medication focusing on skillet HDAC for cutaneous Lymphocyte lymphoma treatment.7 likewise, SAHA has been clinically tried for different sorts of malignant growths including bosom cancer8 and gliomas9 when utilized in blend with traditional disease drugs.

As of late, a benzamide kind of HDACi, MS-275 (6, Entinostat, Figure 1A) has likewise been under numerous clinical preliminaries, strikingly, showing its clinical viability for the therapy of estrogen-positive bosom cancer.10 However for the most part researched for the therapy of malignant growth, a rising quantities of investigations are assessing HDACi for focal sensory system (CNS) sicknesses, like schizophrenia, neurodegenerative problems, seizures, melancholy, and addiction.11−15 One possible benefit of HDAC drugs is the potential for switching strange cell record, as opposed to treating downstream translational endophenotypes. The potential restorative advantages that HDACi could present in CNS issues invigorated us to explore the cerebrum take-up of various notable HDAC inhibitors as likely layouts for the improvement of profoundly strong blood-mind hindrance (BBB) porous HDAC inhibitors for CNS applications. In our underlying examinations, we utilized carbon-11 marked variants of the known HDAC inhibitor drugs, butyric corrosive, valproic corrosive, and 4-phenylbutyric corrosive, to quantify their mind take-up and wholebody pharmacokinetics.16 These medications have CNS applications, especially valproic corrosive, which has been utilized for quite a long time to treat seizure problems. However every one of them have exceptionally restricted BBB porousness. Likewise, we found that the benzamide HDACi, MS-275 (6), has low cerebrum take-up when managed intravenously to nonhuman primates,17 recommending its restriction as a restorative specialist for CNS problems. As of late, Hanson et al.18 likewise showed that the absence of conduct impacts of SAHA is probably going to be because of poor BBB porousness, despite the fact that its restorative potential for CNS applications was recommended by in vitro examinations. Obviously, an efficient way to deal with better anticipate BBB infiltration of little particle tests and medications for CNS therapeutics is required, including that for HDACi.19 Here we report a positron discharge tomography (PET) picture directed blend, radiolabeling, and assessment of profoundly intense and BBB porous HDAC inhibitors focusing on chiefly HDAC isoforms 120 and 221,22 because of their CNS problem importance. We demonstrated our series on the HDAC inhibitor MS275 (6, Figure 1A). Despite the fact that MS-275 isn't BBB penetrable, its somewhat low sub-atomic weight (MW) and nonionic construction at physiological pH give the chance to change various boundaries and the presentation of promptly labelable practical gatherings empowered the quick appraisal of mind take-up utilizing PET. In equal, we surveyed the in vitro strength for HDAC hindrance of the mixtures with the most elevated cerebrum take-up.

RESULTS

Overview. The development of a BBB permeable HDAC inhibitor is based on an iterative plan with four components: in silico structural design and prediction, parallel synthesis and in

Table 1. Inhibition Assay of HDAC1, HDAC2, and HDAC3 (IC_{50}, nM)

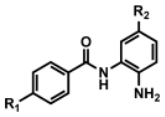

	R_1	R_2	HDAC1[a]	HDAC2	HDAC3
1 (SAHA)	-	-	0.001(0.003)	0.004	0.005
6 (MS-275)	-	H	0.059(0.040)	0.153	0.486
7 (CI-994)	CH_3COCH_2	H	0.045(0.027)	0.031	0.02
8	CH_3COCH_2	2-thienyl	0.002(0.002)	0.002	0.42
9	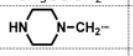	Cl	8.87	6.01	6.5
10	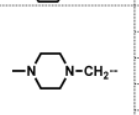	Cl	5.09 (5.5)	1.88	13.3
11		H	0.30	0.62	1.4
12		F	0.22	0.23	-
13		Br	-	-	-
14		I	21.9	10.5	9.8
15	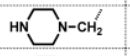	Phenyl	0.006(0.002)	0.023	17.2
16	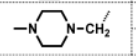	Phenyl	0.005(0.002)	0.022	15.5
17		4-F-C_6H_5	10.2	1.3	2.3
18	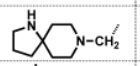	C_6H_5	0.019(0.006)	0.022	17.3
19	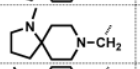	C_6H_5	0.038(0.003)	0.102	9.34
20	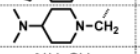	C_6H_5	0.036(0.003)	0.090	22.9
21	NH_2CH_2	H	0.76	2.54	8.21
22	$(CH_3)NHCH_2$	H	0.045(0.005)	0.23	2.55
23	$(CH_3)_2NCH_2$	H	0.47	0.87	0.83
24	NH_2CH_2	C_6H_5	-	-	-
25	$(CH_3)NHCH_2$	C_6H_5	0.025	0.03	13.5
26	$(CH_3)_2NCH_2$	C_6H_5	0.010(0.003)	0.02	5.2
27		4-F-C_6H_5	0.036	0.071	-
28		2-thienyl	0.01(0.003)	0.02	3.76

[a]Recombinant histone deacetylase (the value in parentheses was obtained after 3 h incubation).

vitro HDAC test, radiolabeling, evaluation, and in vivo imaging (Figure 1B). Momentarily, as a beginning stage, four known profoundly strong HDAC drug up-and-comers and their subsidiaries (7, 8, 19) including [11C]MS-275 (6) 17 were named with C-11 and their BBB penetrability was assessed by in vivo PET imaging. This previously set of information was utilized to create beginning rules for primary alteration, contrasted and determined log BB (BB, proportion of mind to plasma centralization of medication in consistent state (Supporting Data (SI) Table 1).23 Then, in light of these outcomes, the following arrangement of mixtures were planned under the thought of equal combination, radiolabeling, and in vitro examine. By and large, three radiolabeled compounds were planned at a time, creating one set for in vivo assessment and producing a quantitative structure−property relationship (QSPR) model (SI). The amassed set of benzamides gave determinant physicochemical properties to be altered for additional streamlining. We utilized mandrill (Papio Anubis) as it is normal to be like human24 and permits more precise blood investigation at various time focuses than rat. Science: Underlying model, Blend, and Radiochemistry. Regardless of the low BBB porousness of [11C]MS-275, the center benzamide structure was picked as a layout for our orderly methodology fluctuating polar surface region (public service announcement), charge, sub-atomic volume (MV) (SI Table 1), and lipophilicity.25 Primarily, substituent change of benzamides was restricted at R1 of phenyl ring An and at R2 of phenyl ring B (Figures 1B and 2) in light of the fact that the two positions have been demonstrated to be basic for HDAC.26 Among different PET isotopes, carbon11 was picked in that its 20.4 min half-life made numerous PET examinations conceivable in 1 day in a similar creature. For simple and quick marking with carbon-11, N-methylation was embraced utilizing [11C]methyl iodide27−29 or [11C]methyl triflate.30 now and

again, N-acetylation was likewise performed with [11C]acetyl chloride.31 At first, we picked two known benzamides,32,33 CI-994 (7, Tacedinaline) and 8, the two of which have low sub-atomic

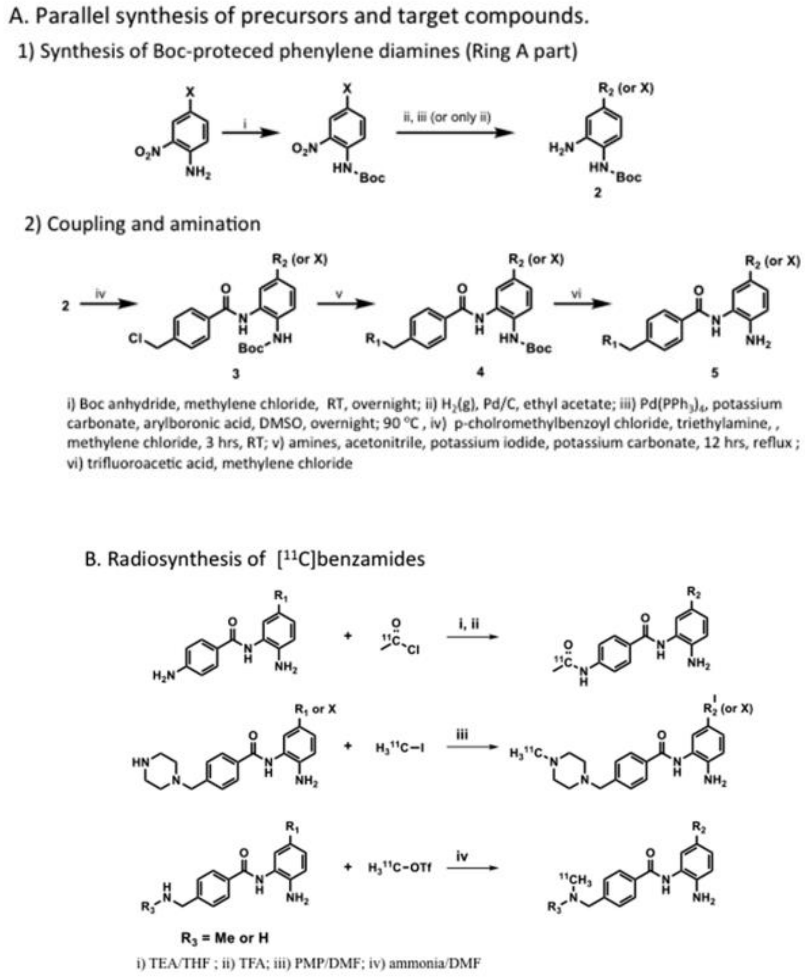

weight

Figure 2. Parallel synthesis and radiolabeling of benzamides.

and sub micromolar HDAC inhibitory activity (Table 1). Carbon-11 versions of these compounds were synthesized by amidation using [11C]acetyl chloride (Figure 2B), which was prepared from [11C]CO2. The spirobicyclic compound 19 was also labeled with [11C]methyl iodide, since its nor-precursor 18 was one of the most potent HDAC1 inhibitors (IC50 = 8 nM) among the known benzamides.26 Precursor and unlabeled standards were synthesized by modification of known procedures in multistep synthesis (SI). However, none of these compounds proved to be BBB permeable in the baboon brain PET imaging study. The first QSPR model built with these compounds (including [11C]MS-275) using the linear cross-correlation matrix revealed that PSA was the main determinant property (r 2 = 0.39) for brain total distribution volume (VT, capacity of the tissue to bind the drug, SI). A set of methylpiperazines varying R1 was selected to reduce PSA in the second round. For the rapid optimization of BBB permeability, we used the parallel synthesis approach as shown in Figure 2.26 Bocprotected phenylenediamines (2 and 3) were coupled with 4-chloromethylbenzoyl choride (4) to provide various benzamides. We set R2 as a labeling position for N-methylation with [11C]methyl iodide or [11C]methyl triflate, introducing a piperazine ring and an N-mono or N-dimethyl amino group. [11C]Methyl iodide or

[11C]methyl triflate was used for Nmethylation of the piperazine group to give high radiochemical yield (40−60%, decay-corrected) in N,N-dimethylformamide (DMF) containing 1,2,2,6,6-pentamethylpiperidine (PMP) within 1 h of radiosynthesis from the end of cyclotron bombardment (Figure 2B). However, N-methylation of benzyl amines, which were chosen as the third set of benzamides, did not provide desired labeled product under these conditions probably due to the reduced nucleophilicity. After exploring many conditions with different combination of bases and solvents, we found that using ammonia as a base gave a moderate yield (10−30%) and sufficient labeled compound for the in vivo imaging study.

In Vitro HDAC Inhibition Assay. Table 1 presents the in vitro results for HDAC inhibition assays of benzamides. This study aims to evaluate the inhibitory efficacy of benzamides, using the well-characterized hydroxamate inhibitor SAHA (1) as a reference standard. Inhibitory activity for HDAC1 was assessed after 1 and 3 hours of incubation with each drug. The substitution of a piperazinylmethyl group at R1 in place of an acetamido group in CI-994 results in a 15-fold reduction in efficacy. Halogen substitution at R1 also decreased potency. The introduction of a phenyl group at R1 significantly enhanced inhibitory activity to the nanomolar range for HDAC1 and -2, but not for -3, suggesting a cation−π electron interaction between the phenyl group and the guanidinium cation of the arginine residue within the deep cavity of the HDAC binding pocket.34.35 Another significant observation was that the in vitro experiment demonstrated that compounds 15 and 16 exhibited rapid and robust inhibitory action comparable to SAHA. The qualities are eliminated by a 4-fluoro substituent on the phenyl ring at R2. The methylated spirobicyclic compound 19 exhibited comparable efficacy to the established nor-precursor compound 18. We also discovered that a very simple amino molecule, 20, was a strong inhibitor of HDAC1 and HDAC2. To decrease PSA and molecular weight for enhanced BBB permeability, the piperazinylmethyl group (compounds 9−17) was substituted with a basic aminomethyl group on R1 (compounds 21−27), while preserving the C-11 labelling position. Analogous to the outcomes seen with piperazine derivatives, potency was restored by including an aromatic group at R1, yielding a potency of 3 nM after 3 hours of in vitro incubation (Table 1). PET Investigation: Blood-Brain Barrier Permeability and Binding Specificity. Positron emission tomography investigations were conducted using 17 carbon-11 labelled benzamides in the baboon brain. Arterial blood was collected throughout the trial duration, and specific samples were analysed using HPLC to quantify the quantity of unmetabolized parent benzamide. The percentage of intact carbon-11 labelled benzamides in plasma was around 60 ± 24% at 10 minutes post-injection (Figure 3A). A series of benzamides including N,N-di- or N-monomethylamino methyl substituents on R2 exhibited a much greater intact percentage (72 ± 5%) (Figure 3A) in comparison to piperazinyl derivatives. MS-275 (6) and CI-994 (7), used in human therapeutic studies, demonstrated a comparatively elevated percentage of intact compounds. A methylated variant of spirobicyclic 19 exhibited a minimal intact percentage at initial time points and a reduced area under the curve (AUC), perhaps aligning with the rapid clearance of its powerful nor-compound, 18, in plasma as reported before (Figure 3B).26 Figure 3C illustrates the cerebral uptake (% injected dosage per cubic centimetre (% ID/cc)) of the chosen carbon-11 labelled benzamides. The carbon-11 labelled CI-994 and the previously described HDAC inhibitor, 8, 32 exhibited little brain absorption, akin to [11C]MS-275 (6). The overall brain absorption of

4-methylpiperazinyl-1-methyl derivatives (10−14, 16, 17) was 4−8 times greater than that of [11C]MS-275 (6) at 15 minutes post-injection. Enhanced efficacy was seen in N,N-dimethylaminomethyl derivatives (23, 26−28), with maximal brain absorption of up to 0.015%ID/cc at 5 minutes post-injection. The total distribution volume (VT), as determined by a one-tissue compartment model, and the AUC ratio of brain to plasma (BAUC/PAUC) for extremely powerful benzamide HDAC inhibitors were computed throughout the 90-minute scan session (Table 2). VT and BAUC/PAUC ranged from 0 to 17 mL/cm3 and 0.1 to 7.5, respectively. Although the values of MS-275 and CI-994 were negligible, the N,N-dimethylamino compounds 26 and 28 exhibited significantly elevated VT and BAUC/PAUC.

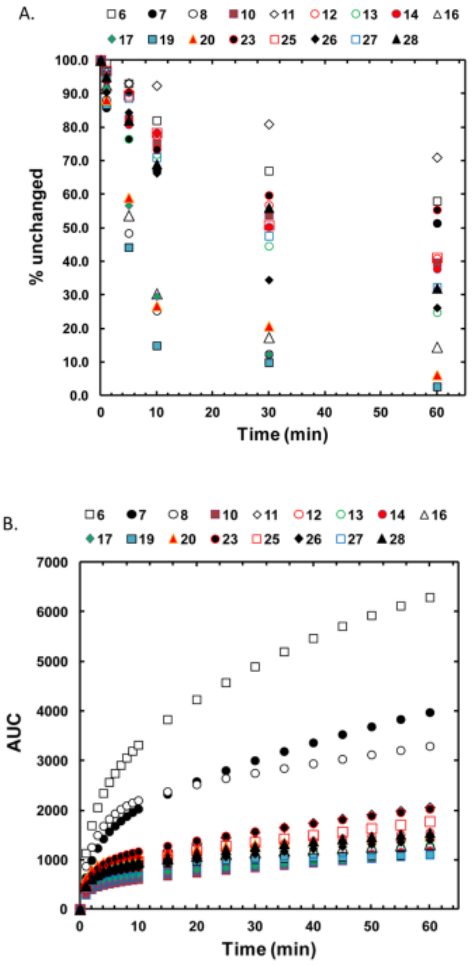

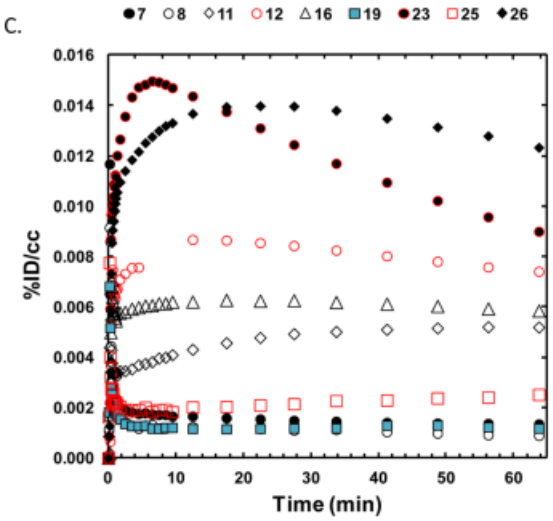

Figure 3. Fraction of unchanged carbon-11 labeled benzamides (A), area under the curves in baboon plasma over 60 m in after time of injection (B), and time−activity curves of global brain uptake for the selected benzamides (C).

Considering both in vitro binding potency and BBB permeability, we chose compound 26 to evaluate binding specificity to brain HDACs. In the baseline studies, the brain

Table 2. Brain Total Distribution Volume and AUC Ratio of Brain to Plasma for Selected [11C]Benzamides

compd	log $D_{7.4}$[a]	cLogP	PSA[b]	V_T (mL/cm^3)	B_{AUC}/P_{AUC}
6, MS-275	1.8	2.5	119.2	0	0.14
7, CI-994	1.0	1.5	98.0	0.41	0.26
8		3.0	98.2	0.22	0.24
16	2.2	3.8	70.2	8.02	3.54
19	4.7	5.4	70.1	4.81	0.93
20		4.8	70.0	1.35	0.77
23		2.2	64.8	5.51	3.93
25		4.0	74.8	2.13	0.90
26	2.1	4.2	64.8	11.96	7.53
28		3.9	64.8	17.81	5.95

[a]Measured. [b]Polar surface area (Å).

distribution of [11C]26 was heterogeneous, showing highest VT in thalamus, cerebellum, and striatum. A repeated baseline study of [11C]26 on the same day in the same animal showed less than 10% of averaged variability of global brain uptake (n = 3). We examined the regional VT change of [11C]26 caused by pretreatment with unlabeled compound 26 (1 mg/kg) or the potent HDAC inhibitor, SAHA (1 mg/kg) (Table 3). The degree of VT reduction ranged 8−24%, compared with the baseline studies in various brain regions.

Table 3. Difference of Total Distribution Volumes (V_T) of Test–Retest and Blocking Study (n = 3)[a]

	test/retest	pretreatment with SAHA	pretreatment with 26
CB	12.6 (±23.5)	−2.5 (±26.8)	−13.4 (±18.4)
TH	−3.9 (±14.6)	−15.4 (±11.1)	−12.9 (±27.0)
TEMP	3.1 (±19.8)	−8.9 (±20.7)	−24.8 (±5.7)
STR	−4.5 (±21.6)	2.5 (±36.0)	3.8 (±48.5)

[a]CB, cerebellum; TH, thalamus; TEMP, temporal cortex; STR, striatum.

DISCUSSION

We present the creation of blood-brain barrier permeable, highly effective HDAC inhibitors using PET in the nonhuman monkey brain. Historically, almost all HDAC inhibitors evaluated in vivo had insufficient blood-brain barrier permeability. Recently, akin to two SAHA-based hydroxamates, we and Shuiyu et al. demonstrated little brain absorption of trichostatin A (TSA)-like hydroxamates and the aryl hydroxamate derivative (KB631) in the baboon brain, respectively. Brain efflux transporters may significantly contribute to these failures, since the hydroxamate medication SAHA is recognised as a P-glycoprotein substrate in in vitro assays.18 Conversely, the cerebral absorption of the benzamide, [11C]MS-275, was not enhanced by the pretreatment with the P-glycoprotein substrate, verapamil.17 To establish a predictive methodology for the creation of BBB-permeable HDAC inhibitors, we implemented a systematic strategy that facilitates rapid iterative feedback on structural modifications from the initial design, utilising highly sensitive image-guided quantification of BBB penetration in a semi-high throughput format. Carbon-11, a transient isotope of carbon (half-life: 20.4 minutes) that undergoes positron emission decay, generating two high-energy photons, may be detected externally by PET imaging. Carbon-11 labelled chemicals and nonhuman monkey PET imaging enable the noninvasive evaluation of medication penetration across the blood-brain barrier, aiding their translation for human uses.40 Owing to the short half-life of carbon-11, a sequential investigation including three distinct [11C]benzamides was efficiently conducted within a single day using the same animal. We integrated this with a QSPR model assessing the efficacy of several molecular descriptors for predicting blood-brain barrier absorption. Two metrics of cerebral uptake relative to plasma were used for the extremely powerful benzamide HDAC inhibitors: the total tissue distribution volume (VT) and the area under the curve (AUC) ratio of brain to plasma (BAUC/PAUC) (Table 2). VT denotes the tissue's ability to bind the drug, while BAUC/PAUC indicates the total drug concentration in the brain during the trial compared to that in plasma for the same duration. A robust linear connection was seen between VT and BAUC/PAUC (R2 = 0.81, SI Figure 1). The metrics of VT and BAUC/PAUC were maximal for compounds 26 and 28 in Table 2, whereas they were minimal for CI-994 (7) and MS-275 (6). Conversely, compound 19 has a superior VT (4.81 mL/cc) in comparison to BAUC/PAUC. The elevated VT is likely associated with the increased log P and log D7.4, suggesting that enhanced lipophilicity leads to diminished brain clearance, resulting in a higher VT. Although the BAUC/PAUC for CI-994 is 0.256, comparable to the previously reported brain/plasma ratio (B/P) of 0.43, we emphasise that the extrapolation of our findings to steady-state B/P is constrained due to the data being derived from bolus IV administration with tracer doses of the labelled compounds.

Based on our prior findings and the anticipated log BB (log(B/P)), the core benzamide structure was chosen and altered as a template for optimising BBB permeability. Charged and high molecular weight derivatives were eliminated. The polar surface area (PSA) is a crucial feature for brain absorption and should not exceed 65 for these benzamides. The elimination of a nitrogen atom by substituting Nmethylpiperazine (16) with a dimethylamino group (26) reduced the PSA from 70.19 to 64.75 and enhanced BBB permeability, resulting in a twofold rise in BAUC/PAUC. The little difference between compound 25 (monomethyl) and compound 26 (dimethyl) led to a sevenfold rise in BAUC/PAUC, which may also be attributed to the quantity of hydrogen bonding donors (HBD). Based on this rationale, we propose that the limited brain permeability of CI-994 (7) is likely due to its elevated PSA (119.16), whereas both molecular volume and PSA forecasted the inadequate brain penetration of MS-275. It became apparent that the PSA (74−107) of all previously reported hydroxamate-based compounds was beyond the acceptable range. In in vitro binding studies, the powerful hydroxamic acid HDAC inhibitor, SAHA, inhibits three isoforms of class I HDACs at low nanomolar concentrations without discernible selectivity. Benzamides exhibited specific inhibitory effect for HDAC1 and HDAC2, which have recently been identified for their therapeutic potential in central nervous system diseases.20 to 22, 43 Notably, several piperazynyl derivatives (17) exhibited moderate selectivity for HDAC2. It is noteworthy that the majority of the benzamides discussed exhibited time-dependent inhibition, suggesting slower kinetics compared to SAHA. Chou et al. and others noted sluggish kinetics coupled with prolonged residence time for many benzamides.44.45 Nevertheless, we discovered that several piperazinyl compounds (15, 16) exhibited rapid HDAC inhibitory action (Table 1). Recent findings indicate that benzamides interact with many HDAC-associated chromatin-modifying complexes, suggesting that binding experiments conducted on pure HDAC may not accurately represent in vivo HDAC activity. However, in contrast to SAHA, CI-994 lacked binding to non-HDAC targets. Our results indicate that the advancement of hydroxamate and benzamide radiotracers shows potential as PET ligands for in vivo measurement of brain HDACs.47 Due to its significant brain uptake and in vitro IC50 values, compound 26 (IC50, 3 nM for HDAC1) was chosen to assess its in vivo binding specificity. In vitro autoradiography demonstrated a relatively high binding density of [3 H]CI-994 in the cerebellum of the mouse brain; nevertheless, the VT decrease of [11C] 26 in the baboon cerebellum was comparable to that seen in the thalamus and striatum, all exhibiting a greater reduction than the cortex. No published information exist about the regional density of HDAC in the monkey brain that may have aided in interpreting the observed geographical variances. The diminished displacement signal may result from the sluggish binding kinetics of benzamides to HDAC, in addition to nonspecific binding interactions. Nonetheless, in the absence of BBB-permeable PET radiotracers, other from [18]FAHA, compound [11C]26 presents a promising blueprint for the advancement of brain-permeable HDAC radiotracers. Significantly, although [18]FAHA, an HDAC substrate, mostly interacts with class II HDACs, benzamides serve as reversible inhibitors of HDAC I, potentially facilitating the assessment of class I HDACs.

CONCLUSION

We express our gratitude to Donald Warner for his contributions to PET operations and to Michael Schueller for his role in cyclotron operations. We recognise the contributions of Tiffany St. Bernard, John Dobbs Jr., and Samuel Wilson, who received support for their synthesis work via the BNL summer internship program. We used two computational chemistry software programs from the Helix Systems at the National Institutes of Health, Bethesda, MD (http://helix.nih.gov) and the Centre for Molecular Modelling (http://cmm.cit.nih.gov).

REFERENCES

(1) Bernal, A. J., and Jirtle, R. L. (2010) Epigenomic Disruption: The Effects of Early Developmental Exposures. Birth Defects Res., Part A 88, 938−944.

(2) Bierne, H., Hamon, M., and Cossart, P. (2012) Epigenetics and Bacterial Infections. Cold Spring Harbor Perspect. Med. 2,x DOI: 10.1101/cshperspect.a010272.

(3) Majumdar, G., Adris, P., Bhargava, N., Chen, H., and Raghow, R. (2012) Pan-Histone Deacetylase Inhibitors Regulate Signaling Pathways Involved in Proliferative and Pro-Inflammatory Mechanisms in H9c2 Cells. BMC Genomics 13, 709−728.

(4) Esteller, M. (2007) Cancer Epigenomics: DNA Methylomes and Histone-Modification Maps. Nat. Rev. Genet. 8, 286−298.

(5) Tsankova, N., Renthal, W., Kumar, A., and Nestler, E. J. (2007) Epigenetic Regulation in Psychiatric Disorders. Nat. Rev. Neurosci. 8, 355−367.

(6) Hyman, S. E. (2012) Target Practice: Hdac Inhibitors for Schizophrenia. Nat. Neurosci. 15, 1180−1181.

(7) Mann, B. S., Johnson, J. R., Cohen, M. H., Justice, R., and Pazdur, R. (2007) FDA Approval Summary: Vorinostat for Treatment of Advanced Primary Cutaneous T-Cell Lymphoma. Oncologist 12, 1247−1252.

(8) Ramaswamy, B., Fiskus, W., Cohen, B., Pellegrino, C., Hershman, D. L., Chuang, E., Luu, T., Somlo, G., Goetz, M., Swaby, R., Shapiro, C. L., Stearns, V., Christos, P., Espinoza-Delgado, I., Bhalla, K., and Sparano, J. A. (2012) Phase I-II Study of Vorinostat Plus Paclitaxel and Bevacizumab in Metastatic Breast Cancer: Evidence for VorinostatInduced Tubulin Acetylation and Hsp90 Inhibition in Vivo. Breast Cancer Res. Treat. 132, 1063−1072.

(9) Lee, E. Q., Puduvalli, V. K., Reid, J. M., Kuhn, J. G., Lamborn, K. R., Cloughesy, T. F., Chang, S. M., Drappatz, J., Yung, W. K. A., Gilbert, M. R., Robins, H. I., Lieberman, F. S., Lassman, A. B., McGovern, R. M., Xu, J. H., Desideri, S., Ye, X. B., Ames, M. M., Espinoza-Delgado, I., Prados, M. D., and Wen, P. Y. (2012) Phase I Study of Vorinostat in Combination with Temozolomide in Patients with High-Grade Gliomas: North American Brain Tumor Consortium Study 04−03. Clin. Cancer Res. 18, 6032−6039.

(10) Yardley, D. A., Ismail-Khan, R. R., Melichar, B., Lichinitser, M., Munster, P. N., Klein, P. M., Cruickshank, S., Miller, K. D., Lee, M. J., and Trepel, J. B. (2013) Randomized Phase II, Double-Blind, PlaceboControlled Study of Exemestane with or without Entinostat in Postmenopausal Women with Locally Recurrent or Metastatic Estrogen Receptor-Positive

Breast Cancer Progressing on Treatment with a Nonsteroidal Aromatase Inhibitor. J. Clin. Oncol. 31, 2128− 2135.

(11) Kilgore, M., Miller, C. A., Fass, D. M., Hennig, K. M., Haggarty, S. J., Sweatt, J. D., and Rumbaugh, G. (2010) Inhibitors of Class 1 Histone Deacetylases Reverse Contextual Memory Deficits in a Mouse Model of Alzheimer's Disease. Neuropsychopharmacol. 35, 870−880.

(12) Golden, S. A., Christoffel, D. J., Heshmati, M., Hodes, G. E., Magida, J., Davis, K., Cahill, M. E., Dias, C., Ribeiro, E., Ables, J. L., Kennedy, P. J., Robison, A. J., Gonzalez-Maeso, J., Neve, R. L., Turecki, G., Ghose, S., Tamminga, C. A., and Russo, S. J. (2013) Epigenetic Regulation of Rac1 Induces Synaptic Remodeling in Stress Disorders and Depression. Nat. Med. 19, 337−344.

(13) Abe, T., and Zukin, R. S. (2008) Epigenetic Targets of Hdac Inhibition in Neurodegenerative and Psychiatric Disorders. Curr. Opin. Pharmacol. 8, 57−64.

(14) Kazantsev, A. G., and Thompson, L. M. (2008) Therapeutic Application of Histone Deacetylase Inhibitors for Central Nervous System Disorders. Nat. Rev. Drug Discovery 7, 854−868.

(15) Price, S., and Dyke, H. J. (2007) Histone Deacetylase Inhibitors: An Analysis of Recent Patenting Activity. Expert Opin. Ther. Pat. 17, 745−765.

(16) Kim, S. W., Hooker, J. M., Otto, N., Win, K., Muench, L., Shea, C., Carter, P., King, P., Reid, A. E., Volkow, N. D., and Fowler, J. S. (2013) Whole-Body Pharmacokinetics of Hdac Inhibitor Drugs, Butyric Acid, Valproic Acid and 4-Phenylbutyric Acid Measured with Carbon-11 Labeled Analogs by Pet. Nucl. Med. Biol. 40, 912−918.

(17) Hooker, J. M., Kim, S. W., Alexoff, D., Xu, Y. W., Shea, C., Reid, A., Volkow, N., and Fowler, J. S. (2010) Histone Deacetylase Inhibitor MS-275 Exhibits Poor Brain Penetration: Pharmacokinetic Studies of [11C]MS-275 Using Positron Emission Tomography. ACS Chem. Neurosci. 1, 65−73.

(18) Hanson, J. E., La, H., Plise, E., Chen, Y. H., Ding, X., Hanania, T., Sabath, E. V., Alexandrov, V., Brunner, D., Leahy, E., Steiner, P., Liu, L., Scearce-Levie, K., and Zhou, Q. (2013) SAHA Enhances Synaptic Function and Plasticity in Vitro but Has Limited Brain Availability in Vivo and Does Not Impact Cognition. PLoS One 8, e69964.

(19) Schreiber, S. L. (2011) Organic Synthesis toward SmallMolecule Probes and Drugs. Proc. Natl. Acad. Sci. U.S.A. 108, 6699− 6702.

(20) Kim, J. Y., Shen, S., Dietz, K., He, Y., Howell, O., Reynolds, R., and Casaccia, P. (2010) HDAC1 Nuclear Export Induced by Pathological Conditions Is Essential for the Onset of Axonal Damage. Nat. Neurosci. 13, 180−189.

(21) Guan, J. S., Haggarty, S. J., Giacometti, E., Dannenberg, J. H., Joseph, N., Gao, J., Nieland, T. J., Zhou, Y., Wang, X., Mazitschek, R., Bradner, J. E., DePinho, R. A., Jaenisch,

R., and Tsai, L. H. (2009) HDAC2 Negatively Regulates Memory Formation and Synaptic Plasticity. Nature 459, 55−60.

(22) Graff, J., Rei, D., Guan, J. S., Wang, W. Y., Seo, J., Hennig, K. M., Nieland, T. J., Fass, D. M., Kao, P. F., Kahn, M., Su, S. C., Samiei, A., Joseph, N., Haggarty, S. J., Delalle, I., and Tsai, L. H. (2012) An Epigenetic Blockade of Cognitive Functions in the Neurodegenerating Brain. Nature 483, 222−226. ACS Chemical Neuroscience Research Article 595 dx.doi.org/10.1021/cn500021p | ACS Chem. Neurosci. 2014, 5, 588−596

(23) Kortagere, S., Chekmarev, D., Welsh, W. J., and Ekins, S. (2008) New Predictive Models for Blood-Brain Barrier Permeability of DrugLike Molecules. Pharm. Res. 25, 1836−1845. (24) Syvanen, S., Lindhe, O., Palner, M., Kornum, B. R., Rahman, O., Langstrom, B., Knudsen, G. M., and Hammarlund-Udenaes, M. (2009) Species Differences in Blood-Brain Barrier Transport of Three Positron Emission Tomography Radioligands with Emphasis on Pglycoprotein Transport. Drug Metab. Dispos. 37, 635−643.

(25) Fan, Y., Unwalla, R., Denny, R. A., Di, L., Kerns, E. H., Diller, D. J., and Humblet, C. (2010) Insights for Predicting Blood-Brain Barrier Penetration of Cns Targeted Molecules Using Qspr Approaches. J. Chem. Inf. Model. 50, 1123−1133.

(26) Kattar, S. D., Surdi, L. M., Zabierek, A., Methot, J. L., Middleton, R. E., Hughes, B., Szewczak, A. A., Dahlberg, W. K., Kral, A. M., Ozerova, N., Fleming, J. C., Wang, H., Secrist, P., Harsch, A., Hamill, J. E., Cruz, J. C., Kenific, C. M., Chenard, M., Miller, T. A., Berk, S. C., and Tempest, P. (2009) Parallel Medicinal Chemistry Approaches to Selective HDAC1/HDAC2 Inhibitor (SHI-1:2) Optimization. Bioorg. Med. Chem. Lett. 19, 1168−1172. (27) Marazano, C., Maziere, M., Berger, G., and Comar, D. (1977) Synthesis of Methyl Iodide-11C and Formaldehyde-11C. Int. J. Radiat. Appl. Instrum. A 28, 49−52.

(28) Link, J. M., Krohn, K. A., and Clark, J. C. (1997) Production of [11C]Ch3I by Single Pass Reaction of [11C]Ch4 with I2. Nucl. Med. Biol. 24, 93−97.

(29) Larsen, P., Ulin, J., Dahlstrøm, K., and Jensen, M. (1997) Synthesis of [11C]Iodomethane by Iodination of [11C]methane. Appl. Radiat. Isot. 48, 153−157.

(30) Jewett, D. M. (1992) A Simple Synthesis of [11C]Methyl Triflate. Int. J. Radiat. Appl. Instrum. A 43, 1383−1385.